AIChE

Application of Flamelet Model to Large-Eddy Simulation of Turbulent Reacting Liquid Flows

Ryoichi Kurose
Dept. of Mechanical Engineering and Science, and Advanced Research Institute of Fluid Science and Engineering, Kyoto University, Yoshida-Honmachi, Sakyo-Ku, Kyoto-shi, Kyoto, Japan

Takenobu Michioka
Environmental Science Research Laboratory, Central Research Institute of Electric Power Industry (CRIEPI), 1646 Abiko, Abiko-shi, Chiba, Japan

Naoki Kohno and Satoru Komori
Dept. of Mechanical Engineering and Science, and Advanced Research Institute of Fluid Science and Engineering, Kyoto University, Yoshida-Honmachi, Sakyo-Ku, Kyoto-shi, Kyoto, Japan

Yuya Baba
Earth Simulator Center (ESC), Japan Agency for Earth-Marine Science and Technology (JAMSTEC), 3173-25 Showa-machi, Kanazawa-ku, Yokohama, Kanagawa, Japan

DOI 10.1002/aic.12328
Published online July 20, 2010 in Wiley Online Library (wileyonlinelibrary.com).

Large-eddy simulations using the flamelet models are applied to turbulent reacting liquid flows and validated by comparing with the experiments. The computations are performed for two reaction conditions, namely a rapid reaction and a moderately fast reaction in a grid-generated turbulent flow. For the flamelet models, both the steady flamelet model and the unsteady Lagrangian flamelet model are tested. A second-order, irreversible, and isothermal reaction is considered. The results show that the flamelet models inherently developed for turbulent combustion are applicable to turbulent reacting liquid flows, provided that the model coefficient in evaluating the subgrid scale variance of mixture fraction in the scale-similarity model is set to be 5.0. The rapid reaction can be adequately predicted by both the steady and unsteady Lagrangian flamelet models, whereas the moderately fast reaction can be predicted only by the unsteady Lagrangian flamelet model which is capable to take slow chemical processes into account. © 2010 American Institute of Chemical Engineers *AIChE J,* 57: 911–917, 2011
Keywords: flamelet model, liquid flow, reaction, large-eddy simulation, turbulence

Introduction

Turbulent reacting liquid flows are widely encountered in many industrial and environmental flows. It is therefore of great importance to develop the numerical simulation technique for them in designing chemical reactors and in predicting turbulent diffusion of chemical pollutants in rivers and ocean.

Large-eddy simulation (LES) is a very attractive tool for numerically simulating turbulent reacting flows with high Reynolds numbers so that a large number of studies have been done for gas flows such as combustion.[1–4] However, the studies on liquid flows are extremely limited. One of the reasons is attributed to the fact that Schmidt number Sc ($= \nu/D$ where ν is the kinematic viscosity and D is the diffusion coefficient) of liquid flows is generally much larger

Correspondence concerning this article should be addressed to R. Kurose at kurose@mech.kyoto-u.ac.jp.

than unity ($Sc \cong 600$) so that Batchelor length scale which is a small-scale variation of passive scalar η_B ($=\eta_K/Sc^{1/2}$) is much smaller than Kolmogorov length scale η_K, unlike gas flows where Sc is around unity. Therefore, more detailed discussion is needed for the application of conventional turbulent reaction models, most of which have been proposed for combustion, to LES of turbulent reacting liquid flows.

Recently, Michioka and Komori[5] proposed a conserved scalar model and a direct closure model for turbulent reacting liquid flows with rapid and moderately fast reactions, respectively, by performing direct numerical simulation (DNS) and LES. The LES results were compared with the measurements.[5–10] What should be remarked in their results most is the modeling of subgrid scale (SGS) variance of a conserved scalar, namely mixture fraction Z, which is an input parameter in using assumed probability density functions for turbulent reaction models. The SGS variance of Z, $\overline{Z''^2}$, is modeled by Cook and Riley[11] under a scale-similarity assumption as

$$\overline{Z''^2} = C_Z \widetilde{Z''^2} = C_Z \left(\widetilde{\overline{Z}^2} - \tilde{\overline{Z}}^2 \right), \tag{1}$$

where C_Z is the model coefficient, Z'' is the fluctuation of Z (i.e., $Z = \overline{Z} + Z''$), and the bar and tilde denote the grid- and test-filtering values, respectively. This assumes that the largest unresolved scales have a structure similar to the smallest resolved scales. Although the value of C_Z is generally believed to be around unity,[12] Michioka and Komori[5] suggested that the adequate value of C_Z for LES of turbulent reacting liquid flows is 5.0. By using this value, their LES results were in good agreement with the measurements.[6–9] However, there remains a problem that their models contain uncertain SGS conditional expectations and do not cover arbitral reaction mechanism and reaction rate as a universal model.

The purpose of this study is to apply other turbulent reaction models, namely the flamelet models[1–3] inherently developed for diffusion combustion, to LES of turbulent reacting liquid flows and validate this approach by comparing with the measurements.[6–9] The marked advantage of the flamelet models is that the reacting flows with a lot of chemical species and steps can be simulated at relatively lower computational costs than others. The computations are performed for a reacting grid-generated turbulent flow with rapid or moderately fast reaction,[6–9] where a second-order, irreversible, and isothermal reaction (A + B $\rightarrow$ 2P) is considered. For the flamelet models, both steady[1,2] and unsteady Lagrangian[11] flamelet models are tested.

Field Description and Numerical Method

Field description

The computational domain and conditions were set to be identical to the experimental ones by Komori et al.[6–9] Figure 1 shows the schematic of the computational domain and conditions. The simulated flow was a grid-generated turbulent liquid flow.[6–9] The computational domain was 520 mm $\times$ 80 mm $\times$ 80 mm in streamwise, vertical, and spanwise directions. At the entrance of the computational domain, a splitter plate with 20-mm length was installed at the center, and a turbulence-generating grid was located at

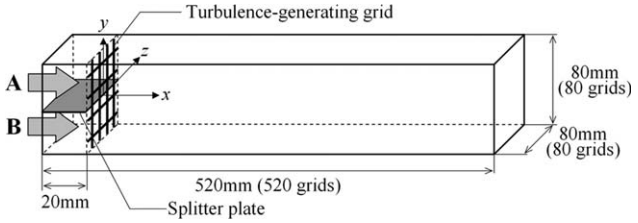

Figure 1. Computational domain and conditions.

20 mm downstream from the entrance. As the round-rod grid with a diameter of 3.0 mm used in the experiments could not be used in the simulation due to the limitations of the coordinate system and the computation cost, the square rod with a thickness of 2.0 mm was set as a turbulence-generating grid. The mesh size of the turbulence-generating grid (i.e., space between the rods) M was 20 mm. The cross-sectionally averaged fluid velocity U_{ave} was 0.25 m/s.

Passive scalar species A and B (i.e., reactants A and B) introduced separately in the upper and lower streams were mixed and reacted in the central region. The reactions presumed were a rapid reaction between acetic acid (species A) and ammonium hydroxide (species B) as

$$CH_3COOH + NH_4OH \rightarrow CH_3COONH_4 + H_2O \tag{2}$$

and a moderately fast reaction between sodium hydroxide (species A) and methylformate (species B) as

$$NaOH + HCOOCH_3 \rightarrow HCOONa + CH_3OH \tag{3}$$

Herein, the initial concentrations of the species A and B for the rapid reaction were 10 mol/m^3 and those for the moderately fast reaction were 100 mol/m^3. The reaction rate constants k_r were 10^8 m^3/(mol s) for the rapid reaction and 0.02 m^3/(mol s) for the moderately fast reaction, respectively.

Large-eddy simulation

For LES using the flamelet models, velocity and mixture fraction Z fields are solved in the physical space and the values of the concentrations of the passive scalar species, namely reactants A and B, and product P at each position are obtained by referring to a database so-called "flamelet library," which is generated beforehand by solving one-dimensional flamelet equations in the Z space. The nondimensional governing equations for LES in the physical space are the filtered conservation equations of mass, momentum (Navier–Stokes (N–S) equation), and Z given by

$$\frac{\partial \overline{U_i}}{\partial x_i} = 0, \tag{4}$$

$$\frac{\partial \overline{U_i}}{\partial t} + \frac{\partial \overline{U_j}\,\overline{U_i}}{\partial x_j} = -\frac{\partial \overline{P}}{\partial x_i} + \frac{1}{Re}\frac{\partial^2 \overline{U_i}}{\partial x_j \partial x_j} - \frac{\partial \tau_{ij}}{\partial x_j}, \tag{5}$$

$$\frac{\partial \overline{Z}}{\partial t} + \frac{\partial \overline{U_j}\,\overline{Z}}{\partial x_j} = \frac{1}{ReSc}\frac{\partial^2 \overline{Z}}{\partial x_j \partial x_j} - \frac{\partial q_{Z_j}}{\partial x_j}, \tag{6}$$

where U_i is the velocity vector, P is the pressure, and the bar denotes the grid-filtering value. It should be noted that the mixture fraction Z can be regarded as reactant A in the

nonreacting case. All quantities are nondimensionalized by using the grid mesh size M and the cross-sectionally averaged fluid velocity U_{ave}. Hence, the Reynolds numbers Re ($=U_{ave}M/\nu$) was 5000 and the Schmidt number was $Sc = \nu/D_Z = 600$. Here, ν is the kinematic viscosity of fluid and D_Z is the diffusivity of Z. It was assumed in this LES that fluid properties of species A, B, P, and Z are equivalent. The subgrid momentum and scalar transport terms τ_{ij} and q_{Zj} were obtained using the dynamic procedure.[13,14] The test filter for the velocity was taken in the streamwise, vertical, and spanwise directions, whereas that for the mixture fraction Z was taken in the streamwise and spanwise directions because the vertical distribution of Z in the central mixing region is awfully inhomogeneous especially in the upstream region.

The governing equations were discretized on a staggered mesh arrangement to construct a finite-difference formation. The spatial derivatives in the filtered N–S and Z equations were approximated by a second-order central difference scheme. The nonlinear terms in the filtered N–S and Z equations are discretized by a second-order fully conservative finite-difference scheme[15] and a QUICK scheme,[16] respectively. A fractional step method and a second-order explicit Runge–Kutta method were used for the time advancement. The slip boundary conditions were imposed on the velocity components on the upper, lower, and side walls because the computational domain was smaller than the experiments, and the convective outflow condition was applied to the outflow boundary in the streamwise direction. The velocity components on the turbulence-generating grid were set to be zero. For the mixture fraction Z, the Neumann condition was imposed on the walls except for the inflow boundary. For the initial flow velocity and mixture fraction Z concentration, the inflow conditions were imposed in the whole region on the upper and lower sides, respectively. The numbers of the grid points used here were $520 \times 80 \times 80$ in the streamwise, vertical, and spanwise directions, respectively. The fine grids were given near the turbulence-generating grid. The number of grid points was determined by comparing the numerical results obtained by computations with various numbers of grid points and grid formations around the turbulence-generating grid. The resolutions are 0.3–1.0 mm in the streamwise direction and 0.8–1.3 mm in the vertical and spanwise directions. Judging from the experiments,[7,8] these are within the inertial subrange in an energy spectrum. Therefore, the use of the subgrid model[13,14] is considered to be adequate. However, the subgrid model for scalar transport may need to be improved because of its high Schmidt number, as discussed later. As new subgrid scalar transport models for the high Schmidt number scalar have been proposed very recently (e.g., Burton[17]), the validation study is our future work.

Flamelet model

The one-dimensional flamelet equations in the Z space for generating the flamelet library is given in a nondimensional form by[1]

$$\frac{\partial \Gamma_i}{\partial \tau} = \frac{\chi}{2}\frac{\partial^2 \Gamma_i}{\partial Z^2} + w_i, \tag{7}$$

where Γ_i is the concentration of species i, χ is the scalar dissipation rate, and w_i is the reaction rate of species i. All quantities are nondimensionalized by using M, U_{ave}, and initial concentration of species A and B ($=\Gamma_0$). τ is the Lagrangian type flamelet time defined by[3]

$$\tau = \int_0^x \frac{1}{<\overline{U}_{\overline{Z}}|\overline{Z}_{st}>(x',t)}\,dx', \tag{8}$$

where $\langle\ \overline{U}_{\overline{Z}}\ |\ \overline{Z}_{st}\rangle$ is the resolved axial velocity of the stoichiometric mixture fraction surface in the physical space. When a second-order, irreversible, and isothermal reaction (A + B $\rightarrow$ 2P) is considered, w_i is expressed as $w_A = w_B = -Da\Gamma_A\Gamma_B$ and $w_P = +2Da\Gamma_A\Gamma_B$. Here, the Damköhler number is defined by $Da = k_r M\Gamma_0/U_{ave}$. For the steady flamelet model,[1,2] as the time variation represented by the left-hand side term is neglected and the value of χ is generally given as a function of Z using a stoichiometric scalar dissipation rate χ_{st} ($=\chi(Z_{st})$ where Z_{st} is the stoichiometric mixture fraction), the values of Γ_i can be tabulated as functions of Z and χ_{st} as Γ_i (Z, χ_{st}). On the other hand, for the unsteady Lagrangian flamelet model,[3], the numerical procedure becomes more complicated. The value of χ is given as a function of Z by referring to the relation of $\overline{\chi}$ and $\overline{Z}$ in the physical space. However, as the distribution of $\chi(Z)$ depends on location and time in the physical space, Γ_i can be tabulated as functions of Z, $\boldsymbol{x}$ and t as Γ_i (Z, $\boldsymbol{x}$, t). Thus, the flamelet library for the unsteady Lagrangian flamelet model is dependent on the configuration and flow behavior of the combustion field of interest, although that of the steady flamelet mode is not.

The values of Γ_i in the Z space and $\overline{\Gamma_i}$ in the physical space are related as

$$\overline{\Gamma_i} = \int_0^1 \Gamma_i(Z,\chi_{st})P(Z)dZ, \tag{9}$$

$$\overline{\Gamma_i}(\boldsymbol{x},t) = \int_0^1 \Gamma_i(Z,\boldsymbol{x},t)P(Z,\boldsymbol{x},t)dZ, \tag{10}$$

for both the steady and unsteady Lagrangian flamelet models, respectively. Here, $P(Z)$ and $P(Z,\boldsymbol{x},t)$ are presumed to follow a β-function, whose shape is determined by the mean Z and the SGS variance of Z, namely $\overline{Z}$ and $\overline{Z''^2}$ (the validity of the β-function is discussed in Michioka and Komori[5]). Therefore, for LES, the table of Γ_i (Z,χ_{st}) was retabulated as $\overline{\Gamma_i}(\overline{Z},\overline{Z''^2},\overline{\chi})$ for the steady flamelet model and that of Γ_i (Z,$\boldsymbol{x}$,t) was retabulated as $\overline{\Gamma_i}(\overline{Z},\overline{Z''^2},\boldsymbol{x},t)$ for the unsteady Lagrangian flamelet model, respectively. Here, $\overline{\chi}$ in the physical space was given as

$$\overline{\chi} = \frac{2}{ReSc}\left(1+\frac{D_t}{D_z}\right)\frac{\partial\overline{Z}}{\partial x_j}\frac{\partial\overline{Z}}{\partial x_j}, \tag{11}$$

where D_t is the SGS turbulent diffusivity evaluated using the dynamic procedure.[4] Equation 7 was implicitly solved with 3000 computational grid points in the Z space. The detailed descriptions of the flamelet models coupled with LES and the generation of the flamelet library are given in Pitsch and Steiner[3] and Baba and Kurose.[18]

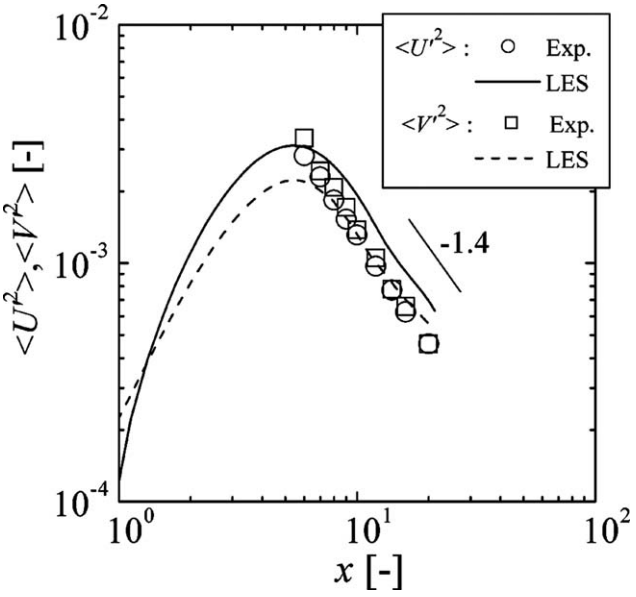

Figure 2. Streamwise distributions of turbulence intensities of longitudinal and vertical velocity fluctuations.

Symbols are experimental results in Ref. 4.

Numerical conditions

The computations were performed for the gird-generated turbulent flow with the rapid or moderately fast reaction. The Damköhler number Da for the rapid and moderately fast reactions were 8.0×10^7 and 0.16, respectively, and these reactions were expressed by both the steady[1,2] and unsteady Lagrangian[3] flamelet models. Although $\overline{Z''^2}$ is often modeled by the scale-similarity model (Eq. 1), this scale-similarity model is known to require a model coefficient C_Z depending on the grid size of the test filter and Reynolds number.[11,12] Therefore, in addition to the scale-similarity model with $C_Z = 0$, 1.0, and 5.0, an alternative approach, in which no model coefficient exists, was also tested here. The algebraic model for $\overline{Z''^2}$ was derived by Pierce and Moin[4] under the assumptions of local homogeneity and local equilibrium for the SGSs as $\overline{Z''^2} = C_2' \Delta^2 \mid \nabla \overline{Z} \mid^2$ where the value of C_Z' is determined dynamically and Δ is the local filter width. This model is referred to as dynamic model, hereafter.

According to the experiments,[7–9] Kolmogorov length and time scales in the simulated isotropic turbulent flow are 130–310 μm and 1.8×10^{-2} to 9.4×10^{-2} s, respectively. On the other hand, the approximate elapse times to the steady state for the computation of the one-dimensional flamelet equations are 1.0×10^{-6} s in the case of the rapid reaction and 300 s in the case of the moderately fast reaction. Although the actual comparison of the Kolmogorov length scale and reactive-diffusive layer thickness cannot be done here by lack of the latter data in the experiments, the flamelet concept is considered to be justified at least for the rapid reaction, as the reaction time scale for the rapid reaction is much faster than that of the Kolmogorov time scale.

Results and Discussion

Flow and mixture fraction fields

The comparisons of the streamwise distributions of turbulence intensities of the longitudinal and vertical velocity fluctuations, $<U'^2>$ and $<V'^2>$, between the LES and the measurements[6–9] are shown in Figure 2. Here, the bracket $\langle\ \rangle$ denotes the time-averaged (mean) value and U_i' is the fluctuation from the mean value (i.e., $U_i = < U_i > + U_i'$). This relation is replaced for LES as $\overline{U}_i = < \overline{U}_i > + \overline{U}_i'$. Therefore, the value of $<U_i'^2>$ is given by taking the SGS fluctuation into account as

$$<U_i'^2> = <\overline{U}_i'^2> + <\overline{U_i''^2}> . \tag{12}$$

where the first and second terms on the right-hand side are the GS and SGS fluctuations, respectively. The second term is neglected, as it is considered that the grid spacing given here is comparable with the Kolmogorov scale, and the effect of the SGS fluctuation is negligible. The profiles of $< U'^2 >$ and $< V'^2 >$ are found to monotonously decrease in the region of $x > 5$, which generally agree with the measured data following a -1.4th power low decay.

Figure 3 displays the distribution of instantaneous mixture fraction on the x–y plane. In addition, the streamwise distributions of the predicted mean-squared mixture fraction fluctuations $< Z'^2 >$ for the scale-similarity model[11] with $C_Z = 0$, 1.0, and 5.0 and the dynamic model[4] are compared with the measured mean-squared concentration fluctuation of reactant A in the no-reaction case[6–9] in Figure 4. In the figure, the scale-similarity and dynamic models are referred to as SSM and DM, respectively. Here, Z' is the fluctuation from the mean value (i.e., $Z = < Z > + Z'$). This relation is replaced for LES as $\overline{Z} = < \overline{Z} > + \overline{Z}'$. It should be noted that these predicted and measured values are supposed to be identical because the mixture fraction Z corresponds to the reactant A in the no-reaction case, as explained earlier. Similar to $< U_i'^2 >$, the value of $< Z'^2 >$ is given by taking the SGS fluctuation into account as

$$<Z'^2> = <\overline{Z}'^2> + <\overline{Z''^2}> . \tag{13}$$

Here, the first and second terms on the right-hand side are the GS fluctuation and SGS fluctuation, respectively. Turbulent

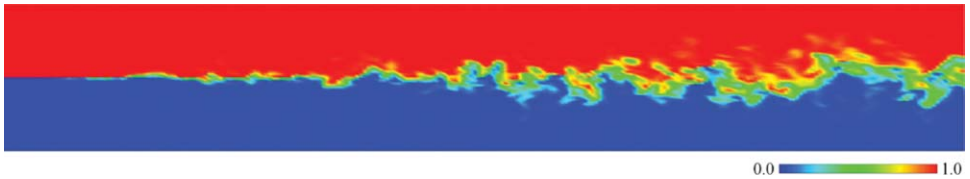

Figure 3. Distribution of instantaneous mixture fraction on the *x–y* plane.

[Color figure can be viewed in the online issue, which is available at wileyonlinelibrary.com.]

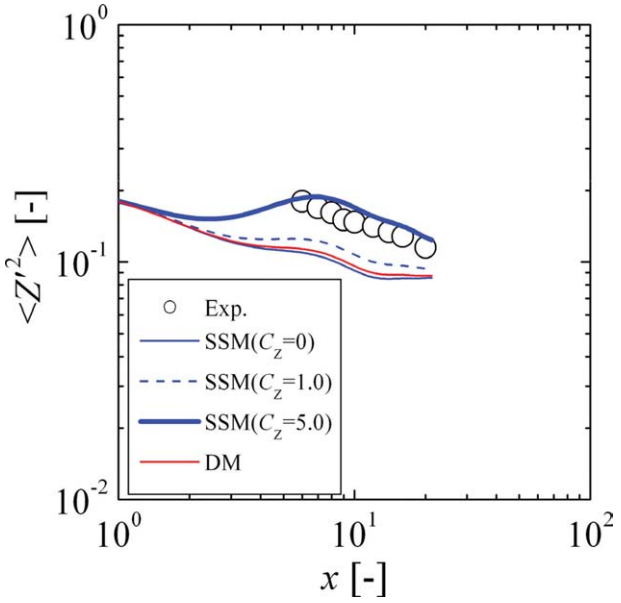

Figure 4. Streamwise distributions of mean-squared mixture fraction fluctuation.

Symbols are experimental results in Ref. 4. [Color figure can be viewed in the online issue, which is available at wileyonlinelibrary.com.]

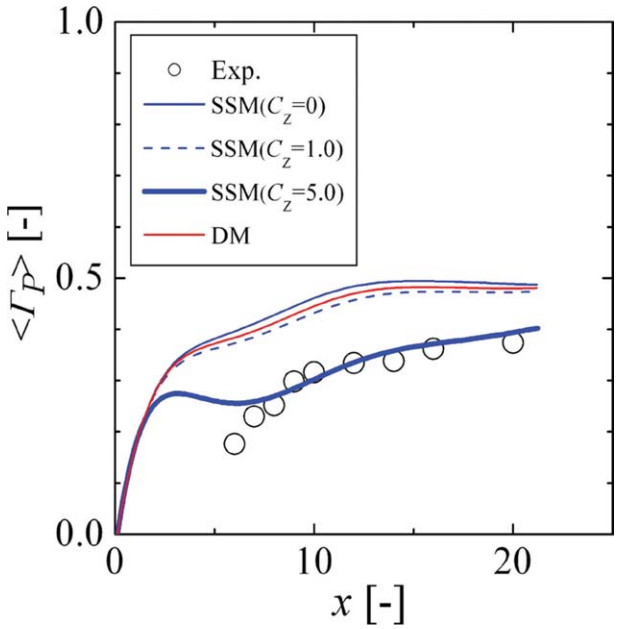

Figure 5. Streamwise distributions of mean concentration of product P obtained by steady flamelet model.

Symbols are experimental results in Ref. 5. [Color figure can be viewed in the online issue, which is available at wileyonlinelibrary.com.]

mixing is found to proceed towards downstream. Although the profile for the scale-similarity model with $C_Z = 0$ is much lower than the measured data, it approaches to them as the value of C_Z increases. Also, the profile is in best agreement with the measured data by using $C_Z = 5.0$, which corresponds to the value proposed by Michioka and Komori.[5] The reason of $C_Z = 5.0$ is speculated in the study of Michioka and Komori[5] in terms of the energy spectrum of concentration fluctuation. That is, as the Schmidt number increases, the viscous–convective subrange in an energy spectrum of concentration fluctuation spreads to the higher wave number region and exists at far smaller scales than the Kolmogorov scale, which causes the increase in the SGS concentration variance. In contrast, the test-filtered concentration variance has almost the same value irrespective of the Schmidt number, as the effect of the Schmidt number appears at smaller scales than the grid scale. As a result, C_Z tends to increase. In fact, Michioka and Komori[5] showed that as the Schmidt number increases, the value of C_Z increases and reaches to 5.0 by performing DNS of isotropic turbulent liquid flows. On the other hand, compared with the scale-similarity model, the profile of $< Z'^2 >$ for the dynamic model is hardly improved. The fact that the value of $< \overline{Z''^2} >$ obtained by the dynamic model tends to be smaller than that by the scale-similarity model with $C_Z = 1.0$ is also reported by Pierce and Moin.[4]

Rapid reaction

The streamwise distributions of mean concentration of product P, $<\Gamma_P> (= <\overline{\Gamma}_P>)$ for the rapid reaction obtained by the steady flamelet model are compared with the measurements[9] in Figure 5 (for reference, the distribution of instantaneous concentration of product P on the x–y plane for the scale-similarity model with $C_Z = 5.0$ is shown in Figure 6). The profiles for the scale-similarity model with $C_Z = 5.0$ are in good agreement with the measured data, and the profiles for the scale-similarity model with $C_Z = 0$ and 1.0 and the dynamic model are larger than that for the scale-similarity model with $C_Z = 5.0$ because of the low value of $< \overline{Z''^2} >$, as shown earlier. Even for the scale-similarity model with $C_Z = 5.0$, the discrepancy from the measurements[9] is marked in the upstream region of around $x = 3$. This is considered due to the fact that the present LES fails to capture the development of the turbulence in the upstream region because of the coarse grids. In fact, as shown in

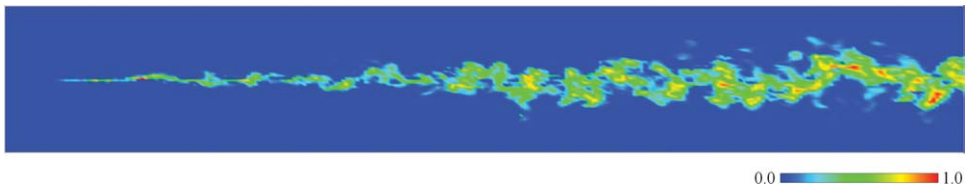

Figure 6. Distribution of instantaneous concentration of product P on the *x–y* plane for rapid reaction obtained by steady flamelet model (scale-similarity model with $C_Z = 5.0$).

[Color figure can be viewed in the online issue, which is available at wileyonlinelibrary.com.]

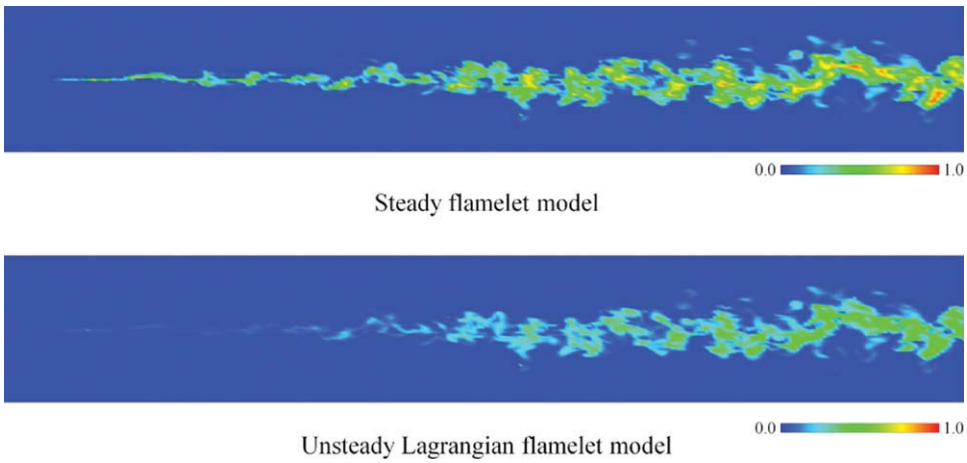

Figure 7. Distributions of instantaneous concentration of product P on the *x–y* plane obtained by steady and unsteady Lagrangian flamelet models (scale-similarity model with $C_Z = 5.0$).

[Color figure can be viewed in the online issue, which is available at wileyonlinelibrary.com.]

Figure 2, the turbulence intensity of vertical velocity fluctuation is underestimated in the upstream region. Although the results are not shown here, the profiles of $< \Gamma_P >$ obtained by the unsteady Lagrangian flamelet model exhibited the similar trends and agreed well with those obtained by the steady flamelet model. This suggests that the adequate value of C_Z of 5.0 is independent of the type of flamelet model.

Moderately fast reaction

Figure 7 displays the distributions of instantaneous concentration of product P on the *x–y* plane for the moderately fast reaction obtained by both the steady and unsteady Lagrangian flamelet models with $C_Z = 5.0$. It is clearly observed that the concentration of product P is much lower for the unsteady Lagrangian flamelet model than for the steady flamelet model. The concentration of product P obtained using the steady flamelet model seems to increase nearly up to the value for the rapid reaction case (Figure 6) in spite of much lower *Da* for the moderately fast reaction case.

The quantitative comparison of the streamwise distributions of $< \Gamma_P >$ obtained by both the steady and unsteady Lagrangian flamelet models are shown in Figure 8, together with the measurements.[9] It is observed that the profiles of $< \Gamma_P >$ obtained by the steady flamelet model exhibit much higher than the measured data. This is because the steady flamelet model cannot be inherently applied to reacting flows with slow reaction rates. On the other hand, the profiles of $< \Gamma_P >$ obtained by the unsteady Lagrangian flamelet model agree well with the measured data. This suggests that the unsteady Lagrangian flamelet model is applicable to LES of turbulent reacting liquid flows with arbitrary reaction rates, although this model possesses an inconvenience that the

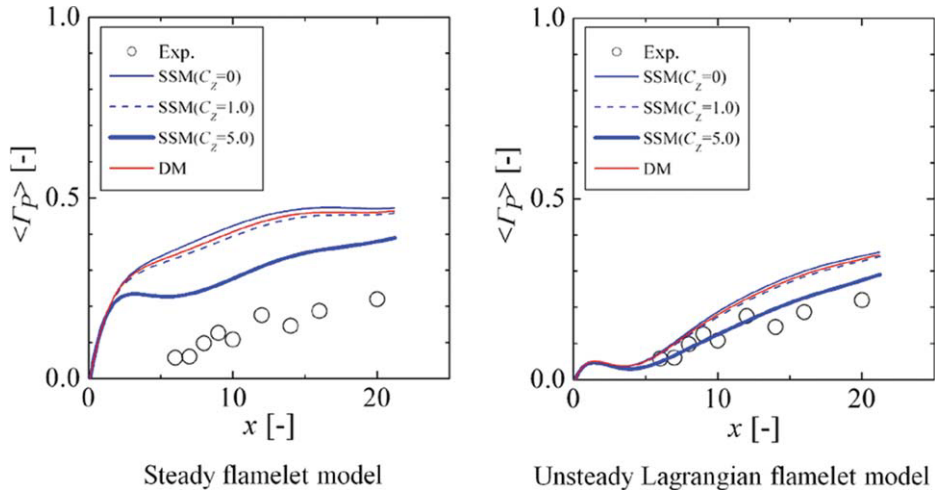

Figure 8. Streamwise distributions of mean concentration of product P obtained by steady and unsteady Lagrangian flamelet models.

Symbols are experimental results in Ref. 5. [Color figure can be viewed in the online issue, which is available at wileyonlinelibrary.com.]

flamelet library is dependent on flow fields. It is also found that the effect of the difference in the model of $\overline{Z''^2}$ is small, namely the deviations of the other models from the scale-similarity model with $C_Z = 5.0$ are small for the moderately fast reaction case, compared with the rapid reaction case. This is attributed to the fact that the reaction is governed by the reaction rate for the moderately fast reaction, whereas it is governed by the turbulent mixing for the rapid reaction.

Conclusions

LES using the flamelet models were applied to turbulent reacting liquid flows and validated by comparing with the experiments. The computations were performed for a reacting grid-generated turbulent flow with rapid or moderately fast reaction, where a second-order, irreversible, and isothermal reaction ($A + B \rightarrow 2P$) was considered. For the flamelet models, both the steady and unsteady Lagrangian flamelet models were tested. The main results obtained in this study can be summarized as follows:

(1) The flamelet models inherently developed for turbulent combustion are applicable to turbulent reacting liquid flows provided that the model coefficient in evaluating the SGS variance of mixture fraction in the scale-similarity model (Cook and Riley[11]), C_Z, is set to be 5.0.

(2) The rapid reaction can be adequately predicted by both the steady and unsteady Lagrangian flamelet models, whereas the moderately fast reaction can be predicted only by the unsteady Lagrangian flamelet model which is capable to take slow chemical processes into account.

Acknowledgments

The numerical simulations were partially carried out by using a parallel supercomputer (NEC:SX-8) of the Center for Global Environment Research, National Institute for Environmental Studies, and Environmental Ministry of Japan.

Literature Cited

1. Peters N. Laminar diffusion flamelet models in non-premixed turbulent combustion. *Prog Energy Combust Sci*. 1984;10:319–339.
2. Peters N. *Turbulent Combustion*. Cambridge: Cambridge University Press, 2000:304.
3. Pitsch H, Steiner H. Large-eddy simulation of a turbulent piloted methane/air diffusion flame (Sandia flame D). *Phys Fluids*. 2000;12: 2541–2554.
4. Pierce CD, Moin P. A dynamic model for subgrid-scale variance and dissipation rate of a conserved scalar. *Phys Fluids*. 1998;10: 3041–3044.
5. Michioka T, Komori S. Large-eddy simulation of a turbulent reacting liquid flow. *AIChE J*. 2004;50:2705–2720.
6. Komori S, Hunt JCR, Kanzaki T, Murakami Y. The effects of turbulent mixing on the correlation between two species and on concentration fluctuation in non-premixed reacting flow. *J Fluid Mech*. 1991;228:629–659.
7. Komori S, Nagata N, Kanzaki T, Murakami Y. Measurements of mass flux in a turbulent liquid flow with a chemical reaction. *AIChE J*. 1993;39:1611–1620.
8. Komori S, Kanzaki T, Murakami Y, Ueda H. Simultaneous measurements of instantaneous concentrations of two species being mixed in a turbulent flow by using a combined laser-induced fluorescence and laser-scattering technique. *Phys Fluids A*. 1989;1:349–352.
9. Komori S, Kanzaki T, Murakami Y. Concentration correlation in a turbulent mixing layer with chemical reactions. *J Chem Eng Jpn*. 1994;27:742–748.
10. Onishi R, Komori S. Thermally-stratified liquid turbulence with a chemical reaction. *AIChE J*. 2006;52:456–468.
11. Cook AW, Riley JJ. A subgrid model for equilibrium chemistry in turbulent flows. *Phys Fluids*. 1994;6:2868–2870.
12. Cook AW. Determination of the constant coefficient in scale similarity models of turbulence. *Phys Fluids*. 1997;9:1485–1487.
13. Moin P, Squires K, Cabot W, Lee S. A dynamic subgrid-scale model for compressible turbulence and scalar transport. *Phys Fluids A*. 1991;3:2746–2757.
14. Bou-Zeid E, Meneveau C, Parlange M. A scale-dependent Lagrangian dynamic model for large eddy simulation of complex turbulent flows. *Phys Fluids*. 2005;17:025105.
15. Morinishi Y, Lund TS, Vasilyev OV, Moin P. Fully conservative higher order finite difference schemes for incompressible flow. *J Comput Phys*. 1998;143:90–124.
16. Leonard BP. A stable and accurate convective modelling procedure based on quadratic upstream interpolation. *Comput Methods Appl Mech Eng*. 1979;19:59–98.
17. Burton GC. The nonlinear large-eddy simulation method applied to $Sc = 1$ and $Sc \gg 1$ passive-scalar mixing. *Phys Fluids*. 2008;20: 035103.
18. Baba Y, Kurose R. Analysis and flamelet modelling for spray combustion. *J Fluid Mech*. 2008;612:45–79.

Manuscript received Mar. 17, 2010, and revision received May 20, 2010.